Utilization of the $Ni_{0.1}Co_{0.9}Fe_2O_4$ Nanocrystals for the Degradation of Crystal Violet

Amina I. Ghoneim[1,], Talaat M. Meaz[1]*

[1] *Physics Department, Faculty of Science, Tanta University, Tanta 31527, Egypt*

Corresponding Authors (*): mona_ghoneim@yahoo.com, amina.ali@science.tanta.edu.eg

Ultra-small $Ni_{0.1}Co_{0.9}Fe_2O_4$ nanocrystals were fabricated via the simple co-precipitation route, then annealed at 900 C /4h, and well-accurately scrutinized by X-ray diffracting strategy (XRD), FT-IR spectral plots, and high resolution transmitting electron microscopy (HRTEM) technique. XRD scrutiny affirmed the emergence of the solitary-phase cubic spinel nanocrystals. The fine crystallite size R average value was 36.265 nm. FT-IR absorption plots displayed the essential absorbing summits which were related to their essential sites and essential bonding types. All parameters were influenced by the subsistence of the Ni2+, Co2+, and Fe3+ cations in these nanocrystals. HRTEM images showed accumulations for the nanoparticles, where the mean particle's size evaluation was 42.9 nm and was slightly bigger than the crystallite size R. Estimation of photocatalytic leverage for Ni0.1Co0.9Fe2O4 Nano-ferrites was obtained through the degradation of Crystal Violet (CV) dye (1 × 10-5 M) in aqueous solution under visible light irradiation using 100 Watt Tungsten lamp fixed at ~ 10 cm distance. Consequently, usage of these ultrafine Ni0.1Co0.9Fe2O4 nanocrystals provides a new marvellous route for the motivation of cost-effective technologies for quite good waste water recycling models, for

raising water quality and for the advancement of fruitful efforts in improving treatment strategies.
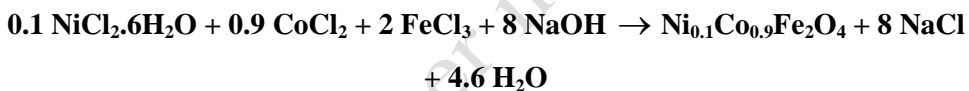
1. Introduction

Photo-catalysts advancement for impure H_2O remediation is a substantial aspect for environmentally ongoing inspection endeavours. Nano-spinels are soft-magnetic semiconducting nanocrystals possessing supreme constancy, and visibly economical; thence these Nano-spinels are facilely fabricated and possess prevalent utilizations in miscellaneous prospects in electromagnets, NTC thermistors, electronical industries, magneto-caloric & magnetic refrigeration, ferrofluids, satellite communications as well as theranostic applications of nanocrystals in medicine. Photo-catalytic effectiveness for dye decadence under visible light photons has exceedingly scrutinized within recent times. Organic dyes are vastly utilized in numerous industries manifesting carcinogenic impress in nature causing counteractive effectiveness on environmental sides. Subsequently, dissociation of such dyes is so essential, where dissociation by photo-catalysis is one of the most effective routes for H_2O up-cleaning [1]. Semiconducting photocatalytic strategy asserted an auspicious methodology for environmentally polluted handling imputing to their entire dissociations from organic contaminations into CO_2 and H_2O at ambient status [2]. Iron oxides and Nano-spinels are utilized as one of expectant and elegant semiconducting nanocrystals; thence they have invigorated splendid inspection vistas assigning to their distinguished merits. Continual attempts have widened to motivate photocatalytic implementation of Iron oxides and Nano-spinels [3]. Inspection attempts in nanoscience have utility towards numerous prospects such as: fabrication, scrutiny of new nanostructures. Vigour of Nanocrystals in fields like telecommunication technology and photo-catalysis is increasing due to the elicited marvellous merits of such nanocrystals [4,5].

Obviously, utilization of Nano-spinel is so efficient in dismantling of organic dyes, where these nanocrystals raise the efficiency of this procedure. This aspect has been early emphasized by [5], utilizing $ZnFe_2O_4$ in this aspect confirming their impress in dye degradation. Thus, current inspection focuses on fabricating new nanocrystals (**$Ni_{0.1}Co_{0.9}Fe_2O_4$** Nano-spinels) and distinguishing their merits. As well as examining their capability in Crystal Violet dissociation. Evaluation of photocatalytic effectiveness for **$Ni_{0.1}Co_{0.9}Fe_2O_4$** Nano-ferrites was obtained through the dissociation of Crystal Violet (**CV**) in aqueous solution under visible light (**VL**) irradiation using 100 Watt Tungsten lamp fixed at ~ 10 cm distance.

2. Experimental Techniques

2.1. Preparation of $Ni_{0.1}Co_{0.9}Fe_2O_4$ nanoparticles

As-fabricated **$Ni_{0.1}Co_{0.9}Fe_2O_4$** Nano-spinels have been fabricated using co-precipitation route according to the formula [6]:

$$0.1\ NiCl_2.6H_2O + 0.9\ CoCl_2 + 2\ FeCl_3 + 8\ NaOH \rightarrow Ni_{0.1}Co_{0.9}Fe_2O_4 + 8\ NaCl + 4.6\ H_2O$$

Detailed Procedure of Co-precipitation have already been reported by Amer, et al 2014 [6]. Then, heated up to 900 ^oC /4h, then cooled to ambient temperature, thereafter the ultrafine dried precipitates were finely ground in a sterilized agate mortar to obtain the Nano-powder [6].

2.2. Characterizations:

Nano-ferrites were scrutinized via GNR APD 2000 Pro X-ray diffractometer step scan type and $CuK\alpha_1$ radiation at wavelength λ = 1.540598 Å. Lattice cons a for **$Ni_{0.1}Co_{0.9}Fe_2O_4$** Nano-spinels was contrived exploiting the expression; $a = d\ (h^2 + k^2 + l^2)^{1/2}$, whilst d is the inter-planar widening elicited by exploiting Bragg's expression; $2\ d \sin\theta = n\ \lambda$, and θ is Bragg's angular position [7]. FT-IR spectra for all nano-samples were explored by using Bruker-Tensor-27-FT-IR - type Spectrometer in the range 200 to 2000 cm^{-1}, at room temperature. Force cons F_1 and F_2 for A- and B-sites was determined using the equation; $F_c = 4\pi^2C^2\nu^2\mu$,

where C is light rapidity, ν is the vibrational frequency and μ is the reduced mass of ions, μ equals about 2.061×10^{-23} gm [8,9]. Moreover, the average nanoparticle size and morphology have been determined by the high resolution transmitting electron microscope of the kind JEOL JEM – 2100 Electron Microscope. UV–vis spectra were registered using SPECTRO UV–VIS DUAL BEAM 8 AUTO CELL UVS-2700 scan-type spectrophotometer in the wavelengths 190–1200 nm at ambient temperature.

2.3. Photocatalytic activity of $Ni_{0.1}Co_{0.9}Fe_2O_4$ nanocrystals:

Photocatalytic features of $Ni_{0.1}Co_{0.9}Fe_2O_4$ nanocrystals were scrutinized by photo-degradation of the simulation of dye waste-water of the crystal violet (**CV**) soln under VL utilizing 100 Watt Tungsten lamp fixed at ~ 10 cm distance, as illuminated in Fig. 1. Aqueous suspension of **CV-dye** (1×10^{-5} **M**) and $Ni_{0.1}Co_{0.9}Fe_2O_4$ nanocrystals as photo-catalysts (0.1 g) was placed in a glass beaker. Before irradiation, each suspension was stirred in dark for 2 h to establish adsorption-desorption equilibrium (between photo-catalyst and dye), followed by VL irradiation utilizing 100 Watt Tungsten lamp fixed at ~ 10 cm distance. At time spans (1 h), 3 mL of suspension was continuously isolated from the beaker, and then filtered to remove the solid powders. Later, the solutions were analysed by the SPECTRO UV–VIS DUAL BEAM 8 AUTO CELL UVS-2700 scan-type spectrophotometer in the wavelengths 190–1200 nm at ambient temperature to obtain the relative concentration variations of the solution. The curve about the concentration variations (**C/C$_o$**) as a function of time was plotted, where **C** presented **CV** concentration at each time span and **C$_o$** was **CV** initial concentration after reaching adsorption-desorption equilibria [10].
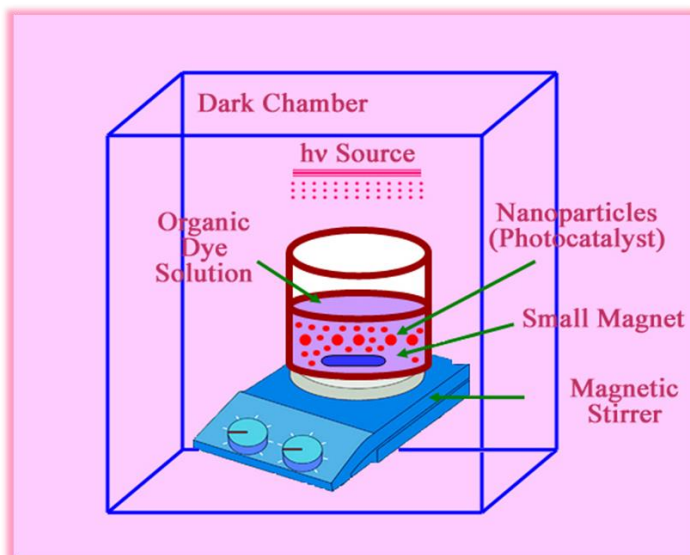
Fig. 1 Schematic illustration of the experimental apparatus setup used for Photo-Degradation mechanism of Crystal Violet (CV) over surface of ultrafine $Ni_{0.1}Co_{0.9}Fe_2O_4$ Nanocrystals.

3. Results and discussion

3.1. X-ray diffracting plots (XRD)

$Ni_{0.1}Co_{0.9}Fe_2O_4$ nanocrystals annealed at 900 C /4h affirmed the complete egress of Nano-spinels monocular-phase which was exquisitely explored by XRD diagrams in Fig. 2. Protruded peaks in XRD diagrams affirm the one-phase Nano-spinel after analogy with JCPDS cards no. 00-001-1121. Plainly, for the ultra-small nano-regime merit of these Nanocrystals thus emerges relatively broader XRD summits in Fig. 2, as further emphasized regarding their fine crystallite sizes for all nanoparticles as indicated in Table 1. Lattice constant a is ranging ≈ 8.479 Å agreeing with early scrutinized work [11]. Elucidated crystallite size R ranges ≈ 36.265 nm, which lies in the Nano-scale ambit.

Obviously, S discloses reliance on both the delicate crystallite size R and X-ray density D_x, and ε relies on R. Since, Nano-spinels have teeny crystallite sizes, so that, they possess large specified surface areas [12]. S and ε estimations are

illuminated in Table 1, which matches well with the posteriorly done appreciations [13]. Unit cell volume V and X-ray densitiy D_x are presented in **Table 1**.
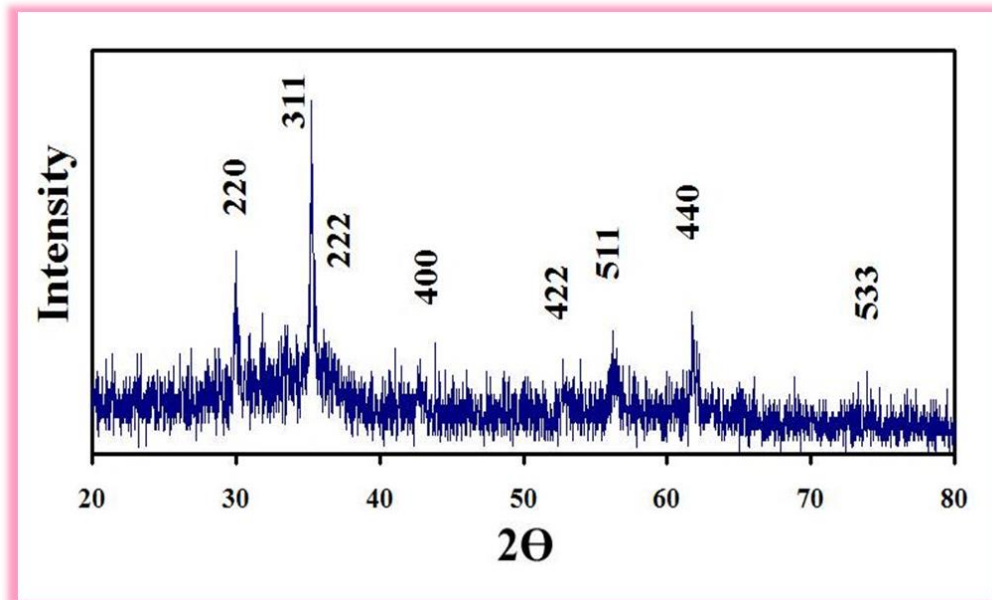

Fig. 2 XRD plots of Nano-spinel **$Ni_{0.1}Co_{0.9}Fe_2O_4$,** heated at 900 ^{o}C.

Table 1 Lattice parameter a, crystallite size R, strain ε, unit cell volume V, X-ray density D_x, specified surface area S, distortion parameter g and dislocation density δ, error = $\pm$ 0.02.

Nano-spinel	a (Å)	R (nm)	ε	V (Å)^3	D_x (gm.cm^{-3})	S (m^2/g)	g	δ (nm^{-2}) × 10^{-2}
$Ni_{0.1}Co_{0.9}Fe_2O_4$	8.479	36.265	- 0.0283	609.45	5.114	32.361	0.0126	0.076

3.2. Structural Phase Analysis

Dimensional cell volume's for these Spinels was contrived utilizing the formulation [14]; $V_{cell} = a^3$. Dimensional cell volume V disclosed a precise value reaching $\approx 609.45 \ (\text{Å})^3$, (**Table 1**).

X-ray density was well contrived utilizing the formula [15]:

$$D_X = \frac{ZM}{N_A V} \qquad (1)$$

, Z is molecules no. per unit cell ($Z = 8$); M is molecular weight and NA is Avogadro's no.

Dislocation density δ was contrived utilizing the expression [16]:

$$\delta = \frac{1}{R^2} \qquad (2)$$

; R is crystallites sizes.

Distortion parameter g was contrived utilizing the formula [16]:

$$g = \frac{\beta_{1/2}}{\tan\theta} \qquad (3)$$

Table 1 discloses dependence of g and δ on R and θ, whilst g and δ rely on interior amendments in Nanocrystal's lattice spacing and oxygen ion concentration [16].

Specified surface area S of Nano-spinels was contrived utilizing [12];

$$S = \frac{6000}{R_{XRD} D_x} \qquad (4)$$

Strain ε of Nano-spinels was contrived utilizing the formula [12];

$$\beta_{1/2} \cos\theta = \frac{0.94\lambda}{R_{XRD}} + 4\varepsilon \sin\theta \qquad (5)$$

Strain ε interior these Nano-spinels relies on cations type and their crystallographic configuration, (Table 1), as well as the protruded crystalline anisotropy [17]. Whilst, specified surface area S revealed a high estimation reaching ≈ 32.361 m^2/g, imputing to the teeny crystallite size R, (**Table 1**).

By plotting the relation between $\beta_{1/2} \cos\theta$ and 4 sinθ for each sample as traight line is obtained its slope gives the strain value. It is seen that ε values are negative, which reveals compressive strain.

3.3. FT-IR Spectral plots

FT-IR spectral plots for **Ni$_{0.1}$Co$_{0.9}$Fe$_2$O$_4$** nanocrystals annealed at 900 C /4h registered from 200 to 2000 cm^{-1} in Fig. 3. Protruded vibrational summits of IR are illuminated in Table 2. Six oscillation summits of ν_1, ν_2, ν_4, ν_A, ν_B and ν_T emerged in FT-IR spectral plots. ν_1 at 605.631 cm^{-1} and ν_2 at 420.471 cm^{-1}, (Table 2), referred to substantial sprawl oscillations of A-occupational allocations ligations; whereas enormous recapture strengths for bond-bending oscillations subsist on B-occupational allocations [18]. Predominately, affirmation of the emersion of Nano-spinel configuration is affirmed by the entity of ν_1 and ν_2. Likewise, it was monitored that vibrational summit at 231.452 cm^{-1} for ν_4 referring to lattice oscillations of Nano-Spinel configuration and it relies on lumps of entirety of A-occupational allocations divalent cations and their ligaments, Fe^{2+} - O^{2-}, Co^{2+} - O^{2-} and/or Ni^{2+} - O^{2-} [6,19]. Ternary vibrational summit ν_T was unfolded around ~ 1629.809 cm^{-1} and was assigned to the retained H_2O in Nano-Crystals [20]. Nonlinear H_2O molecule has 3- substantial oscillational status: symmetric, asymmetric stretching and scissoring oscillation status [20]. Vibrational summits around 898.805 and 1060.82 cm^{-1}, orderly are referring to the vibrational summits ν_A and ν_B. Vibrational summit ν_A refer to coexistence of Fe^{2+}, Co^{2+} amongst the A- sites. Vibrational summit ν_B refer to coexistence of Fe^{4+}-O^{2-} and Ni^{2+}-O^{2-} cations. The protrude of Fe^{4+} cations impute to electronical jumping in-between Fe^{3+} and Co^{2+} cations [6].

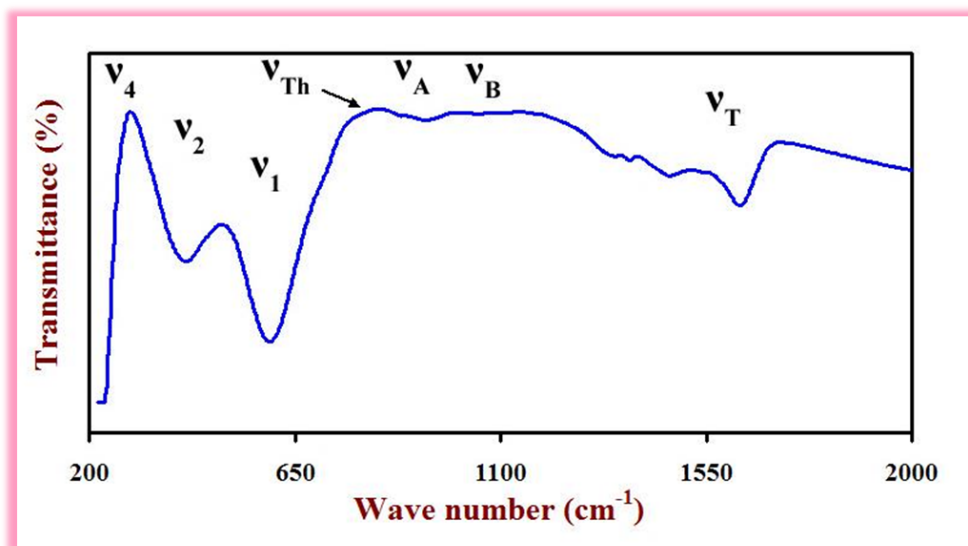**Fig. 3** FT-IR spectral plots of Nano-spinel $Ni_{0.1}Co_{0.9}Fe_2O_4$, heated at 900 ^{o}C.

Table 2 FT-IR vibrational summits positions ν_n; n = 1, 2,…and B, Threshold
frequency ν_{Th}, Threshold energy E_{Th} (eV), Debye temperature Θ_D, Force
con F_1 and F_2, error = ± 0.02.

Nano-spinel	ν_1 (cm^{-1})	ν_2 (cm^{-1})	ν_4 (cm^{-1})	ν_A (cm^{-1})	ν_B (cm^{-1})	ν_T (cm^{-1})	ν_{Th} (cm^{-1})	E_{Th} (eV)	Θ_D (K)	F_1 *10^5 (dyne/cm)	F_2 *10^5 (dyne/cm)
$Ni_{0.1}Co_{0.9}Fe_2O_4$	605.631	420.471	231.452	898.805	1060.82	1629.81	821.61	0.102	737.767	2.686	1.295

Debye temperature was contrived via [21]:

$$\theta_D = \frac{\hbar C \nu_{av}}{k} = 1.438\nu_{av} \quad \text{and} \quad \nu_{AV} = \frac{\nu_1 + \nu_2}{2} \quad (6)$$

, ν_{av} is mean value of wave no's of vibrational summits, $\hbar = h/2\pi$, h is the Plank's
cons, k is Boltzmann's cons, C = 3×10^{10} cm/s; C is light rapidity and $\hbar C / k$ =
1.438 for Nano-spinels [21]: θ_D nearly ≈ 737.767 K and impressed by wave no. of
IR vibrational summits [21].

Concerning specified thermic theorem; the egress of conduction electrons portion (n-type transporters) that fundamentally procure somewhat of thermic potency declining its saucepan, and this bolsters the connotation that conduction impute to electrons, and vice versa. Sill threshold frequency ν_{Th} is subsisting at 821.61 cm^{-1} owing to the transition electrons, while ν_{Th} can be egressed from supreme spot of FT-IR spectral plots [22]; thence, conduction electron no's possess leverage on ν_{Th} and θ_D. Evolved estimation of force cons F_1 and F_2 for A- and B-occupational allocations orderly equals 2.686 $\times 10^5$ and 1.295 $\times 10^5$ dyne/cm, asserting reliance of F_1 and F_2 on oscillational frequencies at these allocations, (Table 2).

Substantially, Threshold energy was contrived utilizing the expression [9]:

$$E_{Th} = hC\nu_{Th} \qquad (7)$$

, where h is Plank's cons, C = 3$\times 10^{10}$ cm/s; C is light rapidity, ν_{Th} is the threshold frequency. Contrived evaluation of ν_{Th} and E_{Th} are presented in Table 2.

Threshold vibrational summit ν_{Th} emerged around 821.61 cm^{-1} shifting towards higher frequencies imputing to the high concentration of Fe^{2+} and Fe^{3+} and as well imputing to the increased hopping status between Fe^{2+}, Fe^{3+} and Fe^{4+} cations as disclosed in the following expression: Fe^{2+} + Fe^{4+} $\leftrightarrow$ Fe^{3+}

Thence, the threshold energy E_{Th} possesses high evaluation going directly on the same demeanour as that of ν_{Th} directly depending on the early estimation of ν_{Th}, (**Table 2**).

3.4. HRTEM images

HRTEM pics of **Ni$_{0.1}$Co$_{0.9}$Fe$_2$O$_4$** Nano-spinels are affirmed in Fig. 4. The pics explore that nanoparticles are accumulated imputing to their magnetic moments. The mean nanoparticle size Z reaches $\approx$ 42.9 nm. It is obvious that, Z evaluation is closer to that of R, where Z is lightly enormous which refer to the

thinning amorphous layer on the nanoparticle's superficies. That is owing to XRD picks only the well-crystalline section interior nanoparticles, whilst HRTEM pics provide complete pics of nanoparticles [11,23].
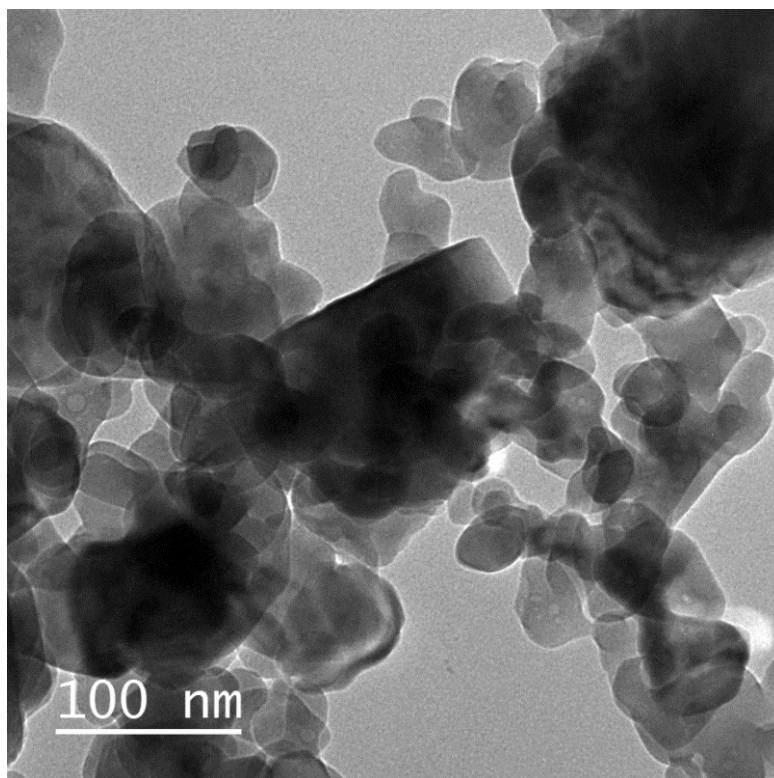

Fig. 4 HTEM pics of Nano-spinel $Ni_{0.1}Co_{0.9}Fe_2O_4$, heated at 900 ^{o}C.

3.5. Photocatalytic features:

Photo-catalytic performance of $Ni_{0.1}Co_{0.9}Fe_2O_4$ Nano-spinels annealed at 900 C /4h for the sequent decolourization of Crystal Violet (**CV**) dye (1×10^{-5} **M**) in aqueous soln under VL irradiation using 100 Watt Tungsten lamp fixed at ~ 10 cm distance, examined under surging of sequent spans of time up to 9 hours, (time duration is 1 hour) were affirmed in Fig. 5. All catalytic degradation reactions followed pseudo-first-ordering kinetics, affirmed by plots of (**C/Co**) versus time (h), as well as the plots of **ln (C/Co)** versus reaction time (h), (Fig. 5). It is explicit that, **CV** concentrations continuously decline with surge of stirring

time emphasizing the photocatalytic activity of these Nano-spinels [24]. Degradation Efficiency was elicited via [25]:

$$Degradation - Efficiency = \left(1 - \frac{C}{C_o}\right) \times 100 \qquad (8)$$

Photo-catalytic efficiency of $Ni_{0.1}Co_{0.9}Fe_2O_4$ Nano-spinels for **CV** degradation was explicitly explored on Fig. 6, proofing surging of their capability and activity in photo-degradation of **CV**, and referring to how high quality will be the treated H_2O by this procedure.
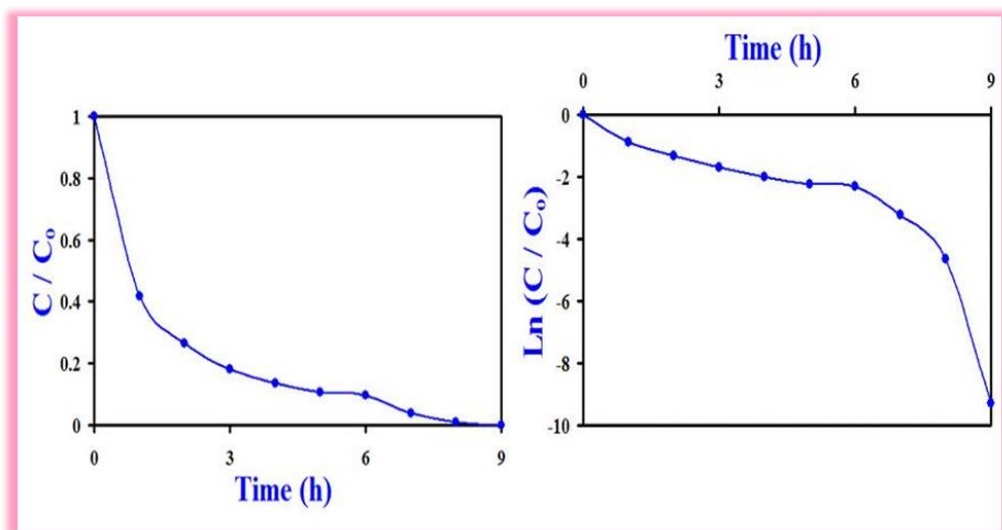

Fig. 5 Photo-Degradation of **CV** (1×10^{-5} **M**) utilizing $Ni_{0.1}Co_{0.9}Fe_2O_4$ Nano-spinels as photo-catalysts, with time duration 1 hour.

Fig. 6 Photo-catalytic efficiency of $Ni_{0.1}Co_{0.9}Fe_2O_4$ Nano-spinels for **CV** (1×10^{-5} **M**) degradation, with time duration 1 hour.

Manifestly, precise utilization of the extremely ultrafine $Ni_{0.1}Co_{0.9}Fe_2O_4$ nanocrystals protrude a new exquisite route for the promotion of echo-friendly technologies for quite delicate waste water reclaiming archetypes, for surging H_2O quality and for the furtherance of effectual exertions in ameliorating treatment mechanisms.

Fig. 7 illuminates the gradual photo-degradation as well as the sequent decolourization of Crystal Violet (**CV**) dye (1×10^{-5} **M**) in aqueous soln under VL irradiation using 100 Watt Tungsten lamp fixed at ~ 10 cm distance, examined under surging of sequent spans of time up to 9 hours, (time duration is 1 hour), utilizing $Ni_{0.1}Co_{0.9}Fe_2O_4$ Nano-spinel as photo-catalyst.

Fig. 7 Gradual photo-degradation and decolourization of Crystal Violet (**CV**) dye (1×10^{-5} **M**) with time duration 1 hour utilizing **Ni$_{0.1}$Co$_{0.9}$Fe$_2$O$_4$** Nano-spinel as photo-catalyst.

Fig. 8 sheds light on the sequent photocatalytic degradation mechanism of Crystal Violet (**CV**) dye (1×10^{-5} **M**) in aqueous soln under VL irradiation using 100 Watt Tungsten lamp fixed at ~ 10 cm distance, inspected under surging of sequent spans of time up to 9 hours, (time duration is 1 hour), utilizing **Ni$_{0.1}$Co$_{0.9}$Fe$_2$O$_4$** Nano-spinel that acts as photo-catalyst.
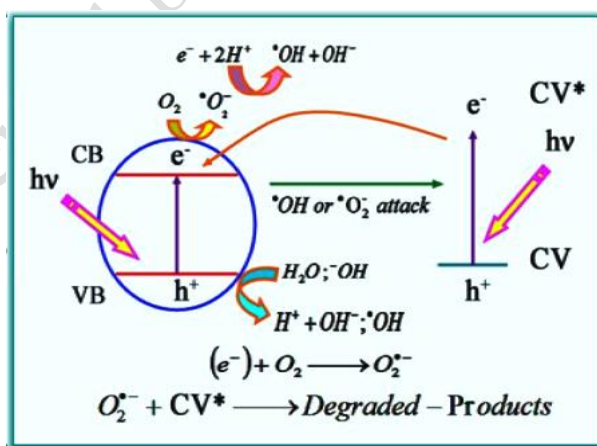

Fig. 8 The sequent photocatalytic degradation mechanism of Crystal Violet (**CV**) dye (1×10^{-5} **M**), utilizing **Ni$_{0.1}$Co$_{0.9}$Fe$_2$O$_4$** Nano-spinel as photo-catalyst, under visible light irradiation, with time duration 1 hour.

4. Conclusion

Ultra-small $Ni_{0.1}Co_{0.9}Fe_2O_4$ nanocrystals were prepared by the simple co-precipitation route, then annealed at 900 C / 4h and precisely distinguished by XRD, FT-IR spectra, and HRTEM techniques. XRD inspection emphasized the egress of single-phase spinel configuration for these nanocrystals. Crystallite size R was ~ 36.265 nm. FT-IR spectral plots emphasized the egress of the two essential spectral summits of Nano-spinels ν_1 and ν_2. Elicited parameters were dependent on Ni^{2+}, Co^{2+}, and Fe^{3+} cations in these Nano-spinels. HRTEM pics provided accumulations for nanoparticles, where average particle size value was 42.9 nm lightly rising than the crystallite size R. Photo-catalysis for $Ni_{0.1}Co_{0.9}Fe_2O_4$ Nano-spinels was acquired through degradation of Crystal Violet (**CV**) dye (1×10^{-5} **M**) in aqueous soln under VL irradiation using 100 Watt Tungsten lamp fixed at ~ 10 cm distance. Explicitly, utilization of $Ni_{0.1}Co_{0.9}Fe_2O_4$ nanocrystals confirmed obvious photo-degradation for **CV**, with excellent efficiency, revealing marvellous strategy for advancement of cost-effective technics for waste H2O recycling models, raising water quality and promoting efforts in treatment systems.

5. References

[1] S Bhukal, S Bansal, S Singhal, Magnetic Mn substituted cobalt zinc ferrite systems: Structural, electrical and magnetic properties and their role in photo-catalytic degradation of methyl orange azo dye, Physica B, 445 (2014) 48–55. http://dx.doi.org/10.1016/j.physb.2014.03.088

[2] T Li, Y Wang, Y He, J Cai, M Luo, L Zhao, Preparation and photocataytic property of $Sr_{0.25}Bi_{0.75}O_{1.36}$ photocatalyst, Mater. Letters 74 (2012) 170–172. doi:10.1016/j.matlet.2012.01.078

[3] J Zeng, J Li, J Zhong, H Yang, Y Lu, G Wang, Improved Sun light photocatalytic activity of α-Fe_2O_3 prepared with the assistance of CTAB, Materials Letters, 160 (2015) 526–528. http://dx.doi.org/10.1016/j.matlet.2015.08.037

[4] CP Yang, PA Smith, J Krupka, TW Button, The losses of microwave ferrites at communication frequencies, J. European Ceramic Society, 27 (2007) 2765-2770. doi:10.1016/j.jeurceramsoc.2006.11.004

[5] E Casbeer, VK Sharma, X-Z Li, Synthesis and Photocatalytic Activity of Ferrites under Visible Light: A Review, Separation and Purification Technology, 87 (2012) 1-14. doi:10.1016/j.seppur.2011.11.034

[6] MA Amer, TM Meaz, SS Attalah, AI Ghoneim, Structural and magnetic characterization of the $Mg_{0.2-x}Sr_xMn_{0.8}Fe_2O_4$ nanoparticles, J. Magn. Magn. Mater., 363 (2014) 60–65. http://dx.doi.org/10.1016/j.jmmm.2014.03.067

[7] SS Thakur, A Pathania, P Thakur, A Thakur, J-H Hsu, Improved structural, electrical and magnetic properties of Mn-Zn-Cd nanoferrites, Ceram. Intern., 41 (2015) 5072-5078. http://dx.doi.org/10.1016/j.ceramint.2014.12.077

[8] KK Bamzai, G Kour, B Kaur, M Arora, RP Pant, Infrared spectroscopic and electron paramagnetic resonance studies on Dy substituted magnesium ferrite, J. Magn. Magn. Mater., 345 (2013) 255–260. http://dx.doi.org/10.1016/j.jmmm.2013.07.002

[9] KB Modi, SJ Shah, NB Pujara, TK Pathak, NH Vasoya, IG Jhala, Infrared spectral evolution, elastic, optical and thermodynamic properties study on mechanically milled $Ni_{0.5}Zn_{0.5}Fe_2O_4$ spinel ferrite, J. Mol. Str., 1049 (2013) 250–262. http://dx.doi.org/10.1016/j.molstruc.2013.06.051

[10] Q Wu, H Yang, H Zhu, Z Gao, Construction of CNCs-TiO_2 heterojunctions with enhanced photocatalytic activity for crystal violet removal, Optik, 179 (2019) 195-206. https://doi.org/10.1016/j.ijleo.2018.10.153

[11] M Rahimi, M Eshraghi, P Kameli, Structural and magnetic characterizations of Cd substituted nickel ferrite nanoparticles, Ceram. Intern., 40 (2014) 15569–15575. http://dx.doi.org/10.1016/j.ceramint.2014.07.033

[12] G Dixit, JP Singh, RC Srivastava, HM Agrawal, Magnetic resonance study of Ce and Gd doped $NiFe_2O_4$ nanoparticles, J. Magn. Magn. Mater., 324 (2012) 479–483. doi:10.1016/j.jmmm.2011.08.027

[13] MA Amer, TM Meaz, SS Attalah, AI Ghoneim, Structural phase transition of as-synthesized Sr–Mn nanoferrites by annealing temperature, J. Magn. Magn. Mater., 393 (2015) 467–478. http://dx.doi.org/10.1016/j.jmmm.2015.06.013

[14] BD Cullity, (1978) Elements of X-ray diffraction, Second Edition, Addison-Wesley Publishing Company, INC, United States of America, Congress catalog No 56-10137.

[15] MA Amer, TM Meaz, SS Attalah, AI Ghoneim, Structural phase transformation of as-prepared Mg–Mn nanoferrites by annealing temperature, Mat. Char. 110 (2015) 197–207, http://dx.doi.org/10.1016/j.matchar.2015.10.032.

[16] V Kumar, Y Ali, RG Sonkawade, AS Dhaliwal, Effect of gamma irradiation on the properties of plastic bottle sheet, Nucl. Instrum. Methods Phys. Res. Sec. B, 287 (2012) 10-14. http://dx.doi.org/10.1016/j.nimb.2012.07.007

[17] N Lenin, RR Kanna, K Sakthipandi, AS Kumar, Structural, electrical and magnetic properties of $NiLa_xFe_{2-x}O_4$ Nanoferrites, Mater. Chem. and Phys. 212 (2018) 385–393. 212:385-393. DOI: 10.1016/j.matchemphys.2018.03.062

[18] BD Cullity, (1972) Introduction to magnetic materials. Addison-Wesley Publishing, Inc., Boston.

[19] M Hashim, KS Alimuddin, SE Shirsath, RK Kotnala, H Chung, R Kumar, Structural properties and magnetic interactions in $Ni_{0.5}Mg_{0.5}Fe_{2−x}Cr_xO_4$ ($0 \leq x \leq 1$) ferrite nanoparticles, Powder Technology, 229 (2012) 37–44. doi:10.1016/j.powtec.2012.05.054

[20] SA Saafan, TM Meaz, EH El-Ghazzawy, MK El Nimr, MM Ayad, M Bakr, A.C. and D.C. conductivity of NiZn ferrite nanoparticles in wet and dry conditions. J. Magn. Magn. Mater., 322 (2010) 2369–2374. doi:10.1016/j.jmmm.2010.02.039

[21] SM Patange, SE Shirsath, KS Lohar, SG Algude, SR Kamble, N Kulkarni, DR Mane, KM Jadhav, Infrared spectral and elastic moduli study of $NiFe_{2-x}Cr_xO_4$ nanocrystalline ferrites. J. Magn. Magn. Mater., 325 (2013) 107–111. http://dx.doi.org/10.1016/j.jmmm.2012.08.022

[22] SM Patange, SE Shirsath, SP Jadhav, VS Hogade, SR Kamble, KM Jadhav, Elastic properties of nanocrystalline aluminium substituted nickel ferrites prepared by co-precipitation method. J. Mol. Str., 1038 (2013) 40–44. http://dx.doi.org/10.1016/j.molstruc.2012.12.053

[23] I Sharifi, H Shokrollahi, Structural, Magnetic and Mössbauer evaluation of Mn substituted Co–Zn ferrite nanoparticles synthesized by co-precipitation, J. Magn. Magn. Mater., 334 (2013) 36–40. http://dx.doi.org/10.1016/j.jmmm.2013.01.021

[24] K Shetty, SV Lokesh, D Rangappa, HP Nagaswarupa, H Nagabhushana, KS Anantharaju, SC Prashantha, YS Vidya, SC Sharma, Designing $MgFe_2O_4$ decorated on green mediated reduced graphene oxide sheets showing photocatalytic performance and luminescence property, Physica B, 507 (2017) 67–75. http://dx.doi.org/10.1016/j.physb.2016.11.021

[25] S Rajoriya, S Bargole, S George, VK Saharan, PR Gogate, AB Pandit, Synthesis and characterization of Samarium and Nitrogen doped TiO_2 photocatalysts for photo-degradation of 4-Acetamidophenol in combination with hydrodynamic and acoustic cavitation, Sep. Pur. Tech., 209 (2019) 254–269. https://doi.org/10.1016/j.seppur.2018.07.036